

# Post-hoc Calibration of Neural Networks by $g$ -Layers

Amir Rahimi <sup>†1</sup>, Thomas Mensink <sup>†2</sup>, Kartik Gupta <sup>1,3</sup>, Thalayasingam Ajanthan <sup>1</sup>,  
Cristian Sminchisescu <sup>2</sup>, Richard Hartley <sup>1,2</sup>

<sup>1</sup>Australian National University <sup>2</sup>Google Research <sup>3</sup>DATA61, CSIRO

<sup>†</sup> Equal Contribution

## Abstract

Calibration of neural networks is a critical aspect to consider when incorporating machine learning models in real-world decision-making systems where the confidence of decisions are equally important as the decisions themselves. In recent years, there is a surge of research on neural network calibration and the majority of the works can be categorized into *post-hoc* calibration methods, defined as methods that learn an additional function to calibrate an already trained base network. In this work, we intend to understand the post-hoc calibration methods from a theoretical point of view. Especially, it is known that minimizing Negative Log-Likelihood (NLL) will lead to a calibrated network on the training set if the global optimum is attained (Bishop 1994). Nevertheless, it is not clear learning an additional function in a post-hoc manner would lead to calibration in the theoretical sense. To this end, we prove that even though the base network ( $f$ ) does not lead to the global optimum of NLL, by adding additional  $g$ -layers and minimizing NLL by optimizing the parameters of  $g$  one can obtain a calibrated network  $g \circ f$ . This not only provides a less stringent condition to obtain a calibrated network but also provides a theoretical justification of post-hoc calibration methods. Our experiments on various image classification benchmarks confirm the theory.

## 1 Introduction

In this paper we consider the problem of calibration of neural networks, or classification functions in general. This problem has been considered in the context of Support Vector Machines (Platt et al. 1999), but has recently been considered in the context of Convolutional Neural Networks (CNNs) (Guo et al. 2017). In this case, a CNN used for classification takes an input  $x \in \mathcal{D}_X$ , belonging to one of  $n$  classes, and outputs a vector  $f(x)$  in  $\mathbb{R}^n$ , where the  $y$ -th component,  $f_y(x)$  is often interpreted as a probability that input  $x$  belongs to class  $y$ . If this value is to represent probabilities accurately, then we require that  $f_y(x) = P(y | f(x))$ . In this case, the classifier  $f$  is said to be *calibrated*, or *multi-class calibrated*.<sup>1</sup>

A well-known condition ((Bishop 1994)) for a classifier to be calibrated is that it minimizes the *cross-entropy* cost

<sup>1</sup>In many papers, e.g. (Kull et al. 2019) and calibration metrics, e.g. ECE (Naeini, Cooper, and Hauskrecht 2015) a slightly different condition known as *classwise calibration* is preferred:  $f_y(x) = P(y | f_y(x))$ .

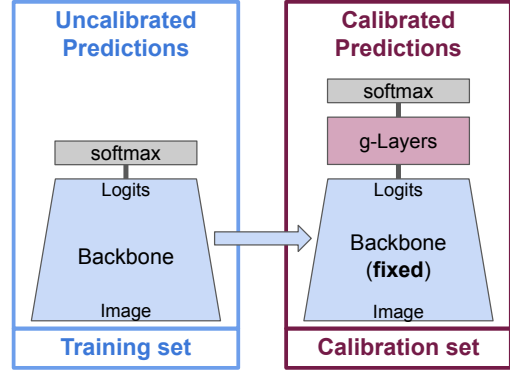


Figure 1: Illustration of  $g$ -layers: (left) a network  $f$  is trained as usual; (right)  $g$ -layers are trained on top of the (fixed)  $f$  using an unseen calibration set. The resulting network  $g(f(x))$  is both *theoretically* as well as *empirical* calibrated.

function, over all functions  $f : \mathcal{D}_X \rightarrow \Delta^{n-1}$ , where  $\Delta^{n-1}$  is the standard probability simplex. If the absolute minimum is attained, it is true that  $f_y(x) = P(y | x)$ . However, this condition is rarely satisfied, since  $\mathcal{D}_X$  may be a very large space (for instance a set of images, of very high dimension) and the task of finding the absolute (or even a local) minimum of the loss is difficult: it requires the network to have sufficient capacity, and also that the network manages to find the optimal value through training. To fulfil this requirement, two networks that reach different minima of the loss function cannot both be calibrated. However, the requirement that a network is calibrated could be separated from that of finding the optimal classifier.

In this paper, it is shown that a far less stringent condition is sufficient for the network to be calibrated; we say that the network is *optimal with respect to calibration* provided no adjustment of the output of the network *in the output space* can improve the calibration (see definition 3). This is a far simpler problem, since it requires that a function between far smaller-dimensional spaces should be optimal.

We achieve optimality with respect to calibration by addition of extra layers at the end of the network and post-hoc training on a hold-out calibration set to minimize the *cross-entropy* cost function, see Fig 1. The extra layers (which we

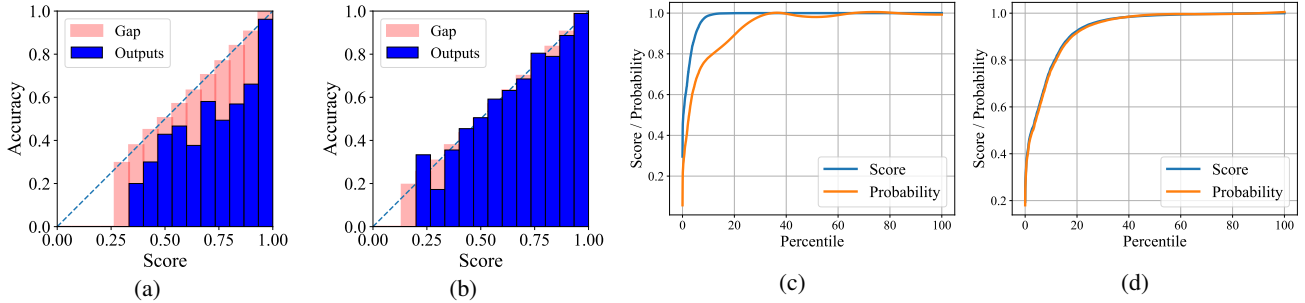


Figure 2: Illustration of ECE and KS calibration metrics for ResNet-110 (Huang et al. 2017) model trained on CIFAR-10 for the *top class*. The uncalibrated network obtains a KS error of 4.8%, and top-1 accuracy of 93.6% on the unseen test set, the calibrated network (with two  $g$ -layers with 32 units each) has an KS error of 0.9%. Reliability diagrams are shown in **a** and **b**, while **c** and **d** show score and probability plotted against fractile for uncalibrated and calibrated networks. If the network is perfectly calibrated, the scores and probability plot will coincide with each other as can be observed in **(d)**.

call  $g$ -layers) take as input the logits (*i.e.* the output before applying the softmax of the original network) and outputs probabilities (*i.e.* with a softmax as final activation). Since the output space of the network is of small dimension (compared to the input of the whole network), optimization of the loss by training the  $g$ -layers is a far easier task.

We conduct experiments on various image classification datasets by learning a small fully-connected network for the  $g$ -layers on a hold-out calibration set and evaluate on an unseen test set. Our experiments confirm the theory that if the calibration set and the test set are statistically similar, our method outperforms existing post-hoc calibration methods while retaining the original accuracy.

## 2 Preliminaries

We consider a pair of joint random variables,  $(X, Y)$ . Random variable  $X$  should take values in some domain  $\mathcal{D}_X$  for instance a set of images, and  $Y$  takes values in a finite set of classes  $\mathcal{Y} = \{1, 2, \dots, n\}$ . The variable  $n$  will refer always to the number of labels, and  $y$  denotes an element of the class set.

We shall be concerned with a (measurable) function  $f : \mathcal{D}_X \rightarrow \mathcal{D}_Z = \mathbb{R}^m$ , and random variable  $Z$  defined by  $Z = f(X) = (f_1(X), f_2(X), \dots, f_m(X))$ . Note that  $\mathcal{D}_Z$  is the same as  $\mathbb{R}^m$ , but we shall usually use the notation  $\mathcal{D}_Z$  to remind us that it is the range of function  $f$ . The distribution of the random variable  $X$  induces the distribution for the random variable  $Z = f(X)$ . The symbol  $z$  will always represent  $f(x)$  where  $x$  is a value of random variable  $X$ . The notation  $x \sim X$  means that  $x$  is a value sampled from the random variable  $X$ . The situation we have in mind is that  $f$  is the function implemented by a (convolutional) neural network. A notation  $P(\cdot)$  (with upper-case  $P$ ) always refers to probability, whereas a lower case  $p$  represents a probability distribution. We use the notation  $P(y | z)$  for brevity to mean  $P(Y = y | Z = z)$ .

A common way of doing classification, given  $n$  classes, is that the neural net is terminated with a layer represented by a function  $q : \mathbb{R}^m \rightarrow \mathbb{R}^n$  (where typically  $m = n$ , but this is not required), taking value  $q(z) = (q_1(z), \dots, q_n(z))$  in  $\mathbb{R}^n$ , and satisfying  $q_i(z) > 0$  and  $\sum_{i=1}^n q_i(z) = 1$ . The set

of such vectors  $q(z)$  satisfying these conditions is called the *standard probability simplex*,  $\Delta^{n-1}$ , or simply the standard (open) simplex. This is an  $n - 1$  dimensional subset of  $\mathbb{R}^n$ . An example of such a function  $q$  is the softmax function defined by  $q_i(z) = \exp(z_i) / \sum_{j=1}^n \exp(z_j)$ .

Thus, the function implemented by a neural net is  $q \circ f$ , where  $f : \mathcal{D}_X \rightarrow \mathcal{D}_Z = \mathbb{R}^m$ , and  $q : \mathbb{R}^m \rightarrow \Delta^{n-1}$ . The function  $q$  will be called the *activation* in this paper. A function such as  $q \circ f : \mathcal{D}_X \rightarrow \Delta^{n-1}$  will be called a *network*. The notation  $q \circ f$  represents the composition of the two functions  $f$  and  $q$ . One is tempted to declare (or hope) that  $q_y(z) = P(y | z)$ , in other words that the neural network outputs the correct conditional class probabilities given the network output. At least it is assumed that the most probable class assignment is equal to  $\operatorname{argmax}_{y \in \mathcal{Y}} q_y(z)$ . It will be investigated how justified these assumptions are. Clearly, since  $f$  can be any function, this is not going to be true in general.

**Loss.** When using the negative log-likelihood (or cross-entropy) loss, the expected loss over the distribution given by the random variables  $(X, Y)$  is

$$\begin{aligned} L(q \circ f, X, Y) &= E_{(x,y) \sim (X,Y)} L(q \circ f, x, y) \\ &= -E_{(x,y) \sim (X,Y)} \log(q_y(f(x))) . \end{aligned} \quad (1)$$

We cannot know the complete distribution of the random variables  $(X, Y)$  in a real situation, however, if the distributions are represented by data pairs  $\mathcal{D} = \{(x_i, y_i)_{i=1}^N\}$  sampled from the distribution of  $(X, Y)$ , then the expected loss is approximated by the empirical loss

$$\begin{aligned} L(q \circ f, \mathcal{D}) &\approx -E_{(x,y) \sim \mathcal{D}} \log(q_y(f(x))) \\ &= -\sum_{i=1}^N \log(q_{y_i}(f(x_i))) . \end{aligned} \quad (2)$$

The training process of the neural network is intended to find the function  $f^*$  that minimizes the loss in Eq 2, given a particular network architecture. Thus  $f^* = \operatorname{argmin}_{f: \mathcal{D}_X \rightarrow \mathbb{R}^m} L(q \circ f, \mathcal{D})$ .

### 3 Calibration

According to theory (see (Bishop 1994)), if a network is trained to minimize the negative log-likelihood over all possible functions, *i.e.*:

$$f^* = \operatorname{argmin}_{f: \mathcal{D}_X \rightarrow \Delta^{n-1}} -E_{(x,y) \sim (X,Y)} \log(f_y(x)) \quad (3)$$

then the network (function  $f^*$ ) is calibrated, in the sense that  $f_y^*(x) = P(y | x)$ , as stated in the following theorem.

**Theorem 1.** Consider joint random variables  $(X, Y)$ , taking values in  $\mathcal{D}_X$  and  $\mathcal{Y}$  respectively, where  $\mathcal{D}_X$  is some Cartesian space. Let  $f : \mathcal{D}_X \rightarrow \Delta^{n-1}$  be a function. Define the loss  $L(f, X, Y) = -E_{(x,y) \sim (X,Y)} \log(f_y(x))$ . If  $f = \operatorname{argmin}_{\hat{f}: \mathcal{D}_X \rightarrow \Delta^{n-1}} L(\hat{f}, X, Y)$  then  $P(y | x) = f_y(x)$ .

This theorem is a fundamental result, but it leaves the following difficulties. Even if the network is trained to completion, or trained with early-stopping, there is no expectation that the loss will be exactly minimized over all possible functions  $f : \mathcal{D}_X \rightarrow \Delta^{n-1}$ . If this were always the case, then research into different network architectures would be largely superfluous.

We show in this paper, however that this is not necessary – a far weaker condition is sufficient to ensure calibration. Instead of the loss function being optimized over all functions  $f : \mathcal{D}_X \rightarrow \Delta^{n-1}$ , it is sufficient that the optimization be carried out over functions  $g : \mathbb{R}^m \rightarrow \mathbb{R}^m$  placed just before the activation function  $q$ . Since the dimension of  $\mathcal{D}_X$  is usually very much greater than the number of classes  $m$ , optimizing over all functions  $g : \mathbb{R}^m \rightarrow \mathbb{R}^m$  is a far simpler task.

**Theorem 2.** Consider joint random variables  $(X, Y)$ , taking values in  $\mathcal{D}_X$  and  $\mathcal{Y}$  respectively. Let  $f : \mathcal{D}_X \rightarrow \mathbb{R}^m$ , and  $Z = f(X)$ . Further, let  $q : \mathbb{R}^m \rightarrow \Delta^{n-1}$  be a submersion. If

$$g = \operatorname{argmin}_{\hat{g}: \mathbb{R}^m \rightarrow \mathbb{R}^m} -E_{(z,y) \sim (Z,Y)} \log(q_y(\hat{g}(z))), \quad (4)$$

then  $P(y | g \circ f(x)) = q_y(g \circ f(x))$ .

The condition that  $q$  is a submersion implies (by definition) that the differential map  $dq : T\mathbb{R}^3 \rightarrow T\Delta^{n-1}$  is a subjection. This required condition of the activation function  $q$  being a submersion is satisfied by most activation functions, including the standard softmax activation.

In broad overview, Theorem 2 is proved by applying Theorem 1 to the function  $q \circ g$  applied to  $u = f(x)$  to show that if  $q \circ g$  is optimal with respect to the loss function, then  $P(y | q \circ g(u)) = q_y(g(u))$ , which is the same as  $P(y | q \circ g \circ f(x)) = q_y(g \circ f(x))$ . The condition that  $q$  be a submersion then allows the condition that  $g \circ q$  is optimal to be “pulled back” to a condition that  $g$  is optimal, in the sense required. The details and proofs are provided in the supplementary material. This theorem leads to the following definition.

**Definition 3.** A network  $g \circ f : \mathcal{D}_X \rightarrow \mathbb{R}^m$  is said to be *optimal with respect to calibration* for a loss-function  $L(\cdot, X, Y)$  and activation  $q : \mathbb{R}^m \rightarrow \Delta^{n-1}$  if Eq 4 is satisfied.

Then Theorem 2 may be paraphrased by saying that the network  $q \circ g \circ f$  (where  $q$  is a submersion) is calibrated if  $g \circ f$  is optimal with respect to calibration.

Theorem 1 and Theorem 2 are given for the negative log-likelihood loss, however this theorem also holds for least-squares error as indicated in (Bishop 1994) and various other cost functions generally known as proper losses (Buja, Stuetzle, and Shen 2005; Reid and Williamson 2010).

**Calibrating partially trained networks.** According to Theorem 2, there is no need for the classifier network  $f_\theta$  to be optimized in order for it to be calibrated. It is sufficient that the last layer of the network (before the *softmax* layer, represented by  $q$ ) should be optimal. Thus, it is possible for the classifier to be calibrated even after early-stopping or incomplete training. Our calibration strategy, presented in section 4, is based on this theorem.

**Classwise and top- $r$  calibration.** Theorem 2 gives a condition for the network to be calibrated in the sense called *multi-class calibration* in (Kull et al. 2019). Many other calibration methods (Kumar, Liang, and Ma 2019; Platt et al. 1999; Zadrozny and Elkan 2002) aim at *classwise calibration*. It can be shown (see the proofs in the supplementary material) that if a classifier is correctly multi-class calibrated, then it is classwise calibrated as well. The converse does not hold.

Furthermore a multi-class calibrated network is also correctly calibrated for the top- $r$  prediction, or within-top- $r$  prediction, *i.e.* the probability of the correct class being one of the top  $r$  predictions equals to the sum of the top  $r$  scores.

Details are as follows. By definition (see also (Kull et al. 2019)) a network  $f$  is said to be multi-class calibrated if  $P(y | z) = z_k$ , where  $z = f(x)$  and  $z_k = f_k(x)$ , which is also our definition of calibration. A network is said to be *classwise calibrated* if for every  $k$  there is a function  $f_k : \mathcal{D}_X \rightarrow [0, 1]$  such that  $P(y | z_k) = z_k$ , so each class is calibrated separately. There is no requirement that  $\sum_k f_k(x) = 1$ . It is shown in our supplementary material that multi-class calibration implies classwise classification, in that the component functions  $f_k$  derived from the function  $f : \mathcal{D}_X \rightarrow \Delta^{n-1}$  are class-calibration functions, though the converse is not true. (This result is not entirely trivial, because in general  $P(y | z_k) \neq P(y | z)$ .)

One can also consider *top- $r$  classification*, or *within top- $r$  classification*, which allows one to determine the probability that the ground-truth  $y$  for a sample is the  $r$ -th highest-scoring classes, or within the top  $r$  highest scoring samples.

In particular, if  $z \in \Delta^{n-1}$ , then we denote the  $r$ -th highest component of the vector  $z$  by  $z^r$ . Note the use of the upper-index to represent the numerically  $r$ -th highest component, whereas  $z_k$  (lower index) is the  $k$ -th component of  $z$ . Given random variables  $Y$  and  $Z = f(X)$ , we can also define the event  $e^{=r}$  to mean that the ground truth  $y \sim Y$  of a sample is equal to the numerically  $r$ -th top component of  $z$ . Similarly,  $e^{\leq r}$  is defined to mean that the ground truth  $y$  is among the top  $r$  scoring classes. We show (see the supplementary

material) that if the network is multi-class calibrated, then

$$P(e^{\leq r} | z) = z^r \quad (5)$$

$$P(e^{\leq r} | z) = \sum_{k=1}^r z^k \quad (6)$$

## 4 Finding a Calibrated Neural Network

Based on Theorem 2 we propose the following strategy to find a calibrated neural network, as also illustrated in Fig 1. Our strategy is to replace function  $f$  by  $g \circ f$ , where  $g$  minimizes the loss function  $L(q \circ g, Z, Y)$  in Eq 4. Then the function  $g \circ f$  will be calibrated. We assume that both  $f$  and  $g$  are implemented by a (convolutional) neural net and proceed as follows:

1. Train the parameters  $\theta$  of a convolutional neural network  $f$  on the *training* set to obtain  $f_\theta$ .
2. Strip any softmax layer (or equivalent) from  $f_\theta$ .
3. Capture samples  $(z, y) \sim (f_\theta(X), Y)$  from a *calibration* set, which should be different from the training set used to train  $f_\theta$ .
4. Train a neural network  $g$  with parameters  $\phi$  on the captured  $\{z, y\}$  samples to minimize Eq 4, providing  $g_\phi$ .
5. The composite network  $g_\phi \circ f_\theta$  is the **calibrated network**.

According to Theorem 2, the output of the composite network  $g \circ f$  will be calibrated, provided that the minimum is achieved when training  $g_\phi$  and that the calibration dataset accurately represents the distribution  $Z = f(X)$ .

It is a far simpler task to train a network  $g_\phi$  to minimize  $L(q \circ g, Z, Y)$  than it is to train  $f_\theta$  to minimize  $L(q \circ f, X, Y)$ , since the dimension of the data  $Z \in \mathbb{R}^m$  is normally far smaller than the dimension of  $\mathcal{D}_X$ . In our experiments, we implement  $g$  as a small multilayer perceptron (MLP) consisting of up to a few dense layers, of dimension no greater than a small multiple of  $m$ . Training time for  $g_\phi$  is usually less than a minute.

**Initialization.** Assuming that function  $f_\theta$  has already been trained to minimize the loss on the training set, when  $g_\phi$  is trained we do not wish to undo all the work that has been done by starting training  $g_\phi$  from an arbitrary (random) point. Therefore, we initialize the parameters of  $g_\phi$  so that initially it implements the identity function. We refer to these layers as *transparent layers*. This is similar to the approach in (Chen, Goodfellow, and Shlens 2015).

An alternative could be to train  $g_\phi \circ f_\theta$  on the training set first, followed by a short period of training on the calibration set, keeping the parameters  $\theta$  fixed. In this case, it is not necessary to initialize the  $g$ -layers to be transparent. The experimental validation of this alternative, however, falls beyond the scope of the current paper.

**Overfitting.** We note that  $f_\theta$  is often well calibrated on the *training* set, but usually poorly calibrated on the *test* set. Similarly, when using a large  $g$ -layer network it is relatively easy to obtain very good calibration on the *calibration* set, however calibration as measured on the *test* set, although far better than the calibration of the original network  $f_\theta$ , is not

always as good. In other words, also the  $g$ -layers are prone to overfitting to the calibration set.

The phenomenon of overfitting to the calibration set has been observed by many authors as far back as (Platt et al. 1999). The lesson from this is that the set used for calibration of the  $g$ -layers should be relatively large. For the CIFAR-10 dataset, we used 45,000 training samples and 5000 calibration samples (standard practice in calibration literature), but a different split of the data may provide better calibration results. In addition, the number of parameters in the  $g$ -layers should be kept low to avoid the risk of overfitting, hence using more than a few layers for  $g_\phi$  seems counter-productive. In practice we (also) add weight decay as regularization.

## 5 Related Work

Calibrating classification functions has been studied for the past few decades, earlier in the context of support vector machines (Platt et al. 1999; Zadrozny and Elkan 2002) and recently on neural networks (Guo et al. 2017). In this literature, it is typically preferred to calibrate an already trained classifier, denoted as *post-hoc calibration*, as it can be applied to any off-the-shelf classifier. Over the past few years, many post-hoc calibration methods have been developed such as temperature scaling (Guo et al. 2017) (as an adaptation of Platt scaling (Platt et al. 1999) for multi-class classification), Bayesian binning (Naeini, Cooper, and Hauskrecht 2015), beta calibration (Kull, Silva Filho, and Flach 2017) and its extensions (Kull et al. 2019) to name a few. These methods are learned on a hold-out calibration set and the main difference among them is the type of function learned and the heuristics used to avoid overfitting to the calibration set. Specifically, temperature scaling learns a scalar parameter while vector or matrix scaling learns a linear transformation of the classifier outputs (Guo et al. 2017). Later, additional regularization constraints such as penalizing off-diagonal terms (Kull et al. 2019) and order-preserving constraints (Rahimi et al. 2020) are introduced to improve matrix scaling. While several practical methods are developed in this regime, it was not clear previously whether learning a calibration function post-hoc would lead to calibration in the theoretical sense. We precisely answer this question and provide a theoretical justification of these methods. Even though, the proof is provided for negative-log loss, it is applicable to any proper loss function (Buja, Stuetzle, and Shen 2005; Reid and Williamson 2010).

We would like to clarify that our theoretical result (similar to (Bishop 1994)) is obtained under the assumption that the calibration set matches the true data distribution (or simply the test set distribution). Similar to the assumption used to train most classifiers. In this regard, there have been various techniques introduced, such as label smoothing (Müller, Kornblith, and Hinton 2019) and data augmentation (Zhang et al. 2018), to avoid overfitting while training a classification (base) network. We believe those techniques are applicable in the calibration context as well.

Dataset	Base Network	Uncalibrated	Temp. Scaling	MS-ODIR	Dir-ODIR	$g$ -Layers				
						1	2	3	4	5
CIFAR-10	ResNet 110	4.751	<b>0.917</b>	0.988	1.076	0.924	0.990	0.954	1.116	1.066
	ResNet 110 SD	4.103	0.362	0.331	0.368	0.317	0.378	0.342	0.307	<b>0.188</b>
	Wide ResNet 32	4.476	0.296	<b>0.284</b>	0.313	0.320	0.296	0.351	0.337	0.420
	DensNet 40	5.493	0.900	0.897	0.969	0.911	1.026	<b>0.669</b>	1.679	1.377
SVHN	ResNet 152 SD	0.853	<b>0.553</b>	0.572	0.588	0.593	0.561	0.579	0.588	0.564
CIFAR-100	ResNet 110	18.481	1.489	2.541	2.335	1.359	1.618	<b>0.526</b>	1.254	-
	ResNet 110 SD	15.833	0.748	2.158	1.901	<b>0.589</b>	1.165	0.848	0.875	-
	Wide ResNet 32	18.784	1.130	2.821	2.000	0.831	<b>0.757</b>	1.900	0.857	-
	DensNet 40	21.157	0.305	2.709	0.775	0.249	<b>0.188</b>	0.199	0.203	-
ILSVRC'12	ResNet 152	6.544	0.792	5.355	4.400	0.776	<b>0.755</b>	0.849	0.757	-
	DensNet 161	5.721	<b>0.744</b>	4.333	3.824	0.881	1.091	0.780	1.105	-

Table 1: KS calibration error (Gupta et al. 2021) (Top-1 in %) comparisons against state-of-the-art post-hoc calibration methods on several image classification datasets, using various network architectures. We vary the number of dense  $g$ -layers in the range 1–5. Each hidden  $g$ -layer has a fixed number of units depending on the number of classes (32, 302, 3002 for 10, 100, 1000 classes respectively). The results show that  $g$ -layers can be trained using NLL effectively reducing the KS error.

Dataset	Base Network	Uncalibrated	Temp. Scaling	MS-ODIR	Dir-ODIR	$g$ -Layers				
						1	2	3	4	5
CIFAR-10	ResNet 110	4.750	1.132	1.052	1.144	1.130	<b>0.997</b>	1.348	1.152	1.219
	ResNet 110 SD	4.113	0.555	0.599	0.739	0.807	0.809	0.629	0.674	<b>0.503</b>
	Wide ResNet 32	4.505	0.784	0.784	0.796	<b>0.616</b>	0.661	0.634	0.669	0.670
	DensNet 40	5.500	0.946	1.006	1.095	1.101	1.037	<b>0.825</b>	1.729	1.547
SVHN	ResNet 152 SD	0.862	0.607	0.616	0.590	0.638	<b>0.565</b>	0.589	0.604	0.648
CIFAR-100	ResNet 110	18.480	2.380	2.718	2.896	2.396	2.334	<b>1.595</b>	1.792	-
	ResNet 110 SD	15.861	<b>1.214</b>	2.203	2.047	1.219	1.405	1.423	1.298	-
	Wide ResNet 32	18.784	1.472	2.821	1.991	1.277	<b>1.096</b>	2.199	1.743	-
	DensNet 40	21.156	0.902	2.709	0.962	0.927	0.644	0.562	<b>0.415</b>	-
ILSVRC'12	ResNet 152	6.543	2.077	5.353	4.491	2.025	2.051	<b>1.994</b>	2.063	-
	DensNet 161	5.720	1.942	4.333	3.926	1.952	1.978	<b>1.913</b>	1.931	-

Table 2: Expected calibration error (ECE) (Naeini, Cooper, and Hauskrecht 2015) (Top-1 in %) comparisons against state-of-the-art post-hoc calibration methods on several image classification datasets using various network architectures. We vary the number of dense  $g$ -layers in the range 1–5. Each hidden  $g$ -layer has a fixed number of units depending on the number of classes (32, 302, 3002 for 10, 100, 1000 classes respectively). The results show that  $g$ -layers can be trained using NLL effectively reducing the ECE error.

## 6 Experiments

### Experimental setup

For our experimental validation we calibrate deep convolutional neural networks trained on the CIFAR-10/CIFAR-100 (Krizhevsky 2009), SVHN (Netzer et al. 2011) and ILSVRC'12 (Russakovsky et al. 2015) datasets. For the base network  $f$  we use pre-trained models of different architectures: ResNet (He et al. 2016), ResNet Stochastic Depth (Huang et al. 2016), DenseNet (Huang et al. 2017), and Wide ResNet (Zagoruyko and Komodakis 2016). For most of the experiments we use the pre-trained models also used in (Kull et al. 2019).

**Initialization.** The proposed  $g$ -layers are initialized with transparent layers so that at initialization they represent an identity mapping similar to the idea in (Chen, Goodfellow, and Shlens 2015). Preliminary results have shown that

this transparent initialisation is necessary to train the  $g$ -layers from the relatively small calibration set. Especially for datasets with many classes the accuracy will drop significantly when normal random initialised weights are used.

**Training.** The  $g$ -layers are trained on a *calibration* set (not used for training base networks nor for evaluation). The hyper-parameters for learning (learning rate and weight decay) are determined using 5-fold cross validation on the calibration set. The best results are used to train the  $g$ -layers on the full calibration set. For all models (cross-validation and final calibration) early stopping is used based on the negative log-likelihood of the current training set.

**Evaluation.** To evaluate the  $g$ -layers, the calibration error is evaluated on the *test* set. While our theory as well as our approach guarantees multi-class calibration (*c.f.* section 3), in the calibration literature (Guo et al. 2017; Kull

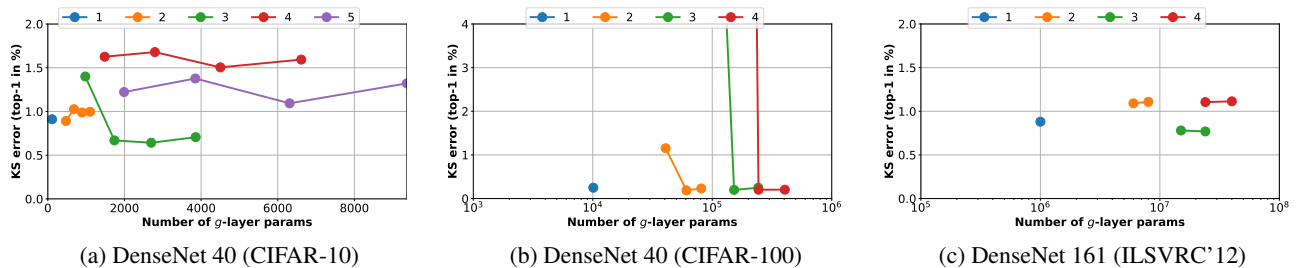


Figure 3: Plots of KS error (top-1 in %) as a function of the number of parameters in the  $g$ -layer networks. For the  $g$ -layers, the number of dense layers is varied (indicated by the different colors) and number of dense units per layer. Here we use  $\{2, 3, 4, 5\}$  units per class for CIFAR-10,  $\{2, 3, 4\}$  for CIFAR-100, and  $\{3, 4\}$  for ILSVRC'12.

Dataset	Base Network	Uncalibrated	$g$ -Layers
CIFAR-10	ResNet 110	1.066	0.283
	ResNet 110 SD	0.918	0.108
	Wide ResNet 32	0.995	0.121
	DensNet 40	1.234	0.174
SVHN	ResNet 152 SD	0.188	0.138
CIFAR-100	ResNet 110	3.299	0.336
	ResNet 110 SD	2.904	0.234
	Wide ResNet 32	3.459	0.462
	DensNet 40	3.877	0.169
ILSVRC'12	ResNet 152	1.155	0.329
	DensNet 161	1.040	0.306

Table 3: Multi-class calibration as measured by the average Top-10 KS metric. Across all networks and datasets  $g$ -layers significantly improve the multi-class calibration.

et al. 2019), the standard practice is to measure the calibration of top-1 predictions (or generally classwise calibration).

We measure top-1 calibration error using Expected Calibration Error (ECE) (Naeini, Cooper, and Hauskrecht 2015) and Kolmogorov-Smirnov calibration error (KS-error) (Gupta et al. 2021). While ECE is a widely used metric, a known weakness is its dependence on histograms (see Fig 2 (a) and (b)) which is deemed as a weakness since the final error depends on the chosen histogram binning scheme. ECE might be particularly unsuitable on deep networks trained on small datasets such as CIFAR-10, since over 90% of scores are over 0.9, and hence lie in a single bin (see Fig 2 (c), which plots the scores versus fractile).

The KS-error (Gupta et al. 2021) computes the maximum difference between the cumulative predicted distribution and the true cumulative distribution. If the network is consistently over- or under-calibrated, which is usually the case, then the KS-error measures the (empirical) expected absolute difference between the score  $q_i(g(f(x)))$  and the probability  $P(i | q_i(g(f(x))))$ , where  $i = \operatorname{argmax}_{y \in \mathcal{Y}} q_y(g(f(x)))$ . The cumulative distributions also provides visualizations similar to reliability diagrams, see e.g. Fig 4.

## Results

We first provide an experimental comparison with other post-hoc calibration methods on the dataset used. Then, we discuss in more depth the between the number of parameters in  $g$ -layers and overfitting with respect to calibration for a given dataset. In short, as predicted by our theory, if overfitting to the calibration set is reduced in practice, learning complete  $g$ -layers lead to superior calibration. Nevertheless, heuristics for mitigating overfitting such as using larger calibration set and increased regularization (dropout, weight-decay, etc.) are relevant and the best approach to avoid overfitting with respect to calibration remains an open question.

**Comparisons to other methods.** In this set of experiments we compare  $g$ -layer calibration to several other calibration methods, including temperature scaling (Guo et al. 2017), MS-ODIR (Kull et al. 2019), and Dir-ODIR (Kull et al. 2019). To provide the calibration results using the baseline methods, we use the base models and implementation of (Kull et al. 2019). Since, we do not need to retrain the base models, we train  $g$ -layers on top of the pre-trained models.

We train  $g$ -layers with different number of dense layers, in the range from 1–5. The size of the hidden  $g$ -layers is fixed to  $H = 3 \times C + 2$ , where  $C$  is the number of classes in the dataset. This satisfies the requirement for the transparent initialisation that  $H > 2C$ . In practice this means that the number of weights in  $g$ -layers scale cubic with the number of classes, e.g. the 3-layer network for ILSVRC'12 contains 15M weights, while the 4-layer network has 24M.

The performance is measured using KS-Error, in Table 1, and ECE, in Table 2. We observe that the proposed  $g$ -layers achieve at least comparable calibration performance to the current state-of-the-art methods, but often (significant) better. In general there is a negligible effect on the accuracy ( $\pm 0.5\%$ ) of the base network, see supplementary material for full results.

We would like to point out that all the compared methods belong to the post-hoc calibration category and can be thought of as special cases of our method (that is learning a  $g$ -function). The main difference between these methods is the allowed function class while optimizing the  $g$ -layers, which can be thought of as a technique to avoid overfitting on a small calibration set.

For our *dense*  $g$ -layers holds that the 5-fold cross valida-

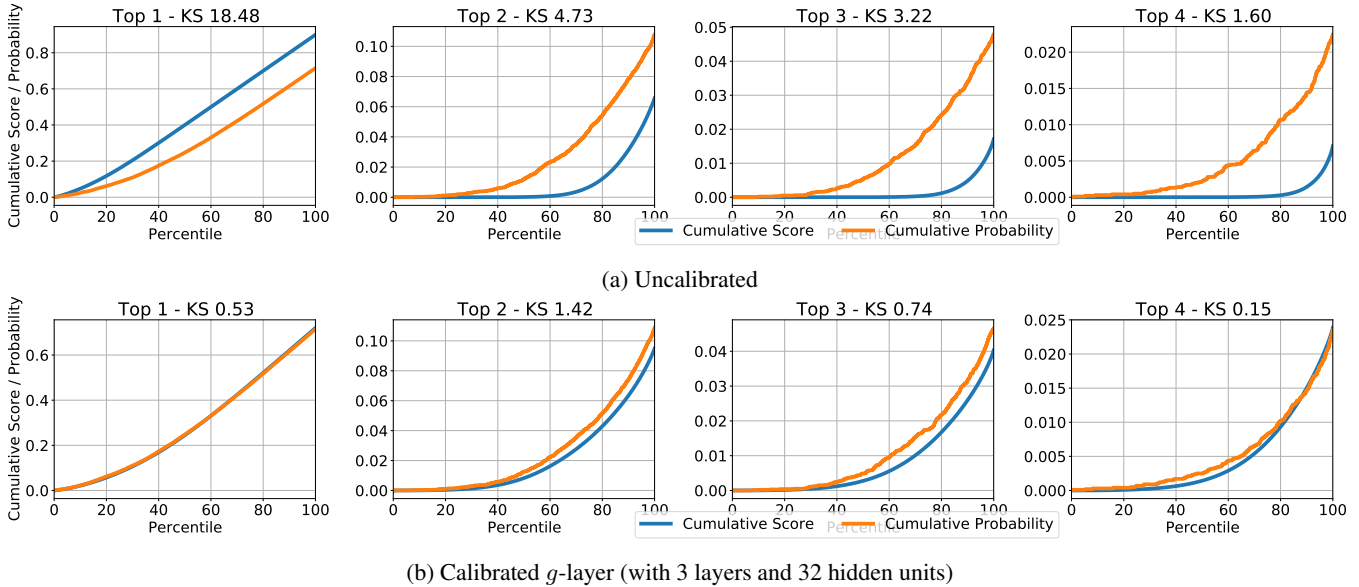


Figure 4: Comparison of the KS error of the Top-1 to Top-4 classes between the uncalibrated ResNet 110 model (*top*) and the calibrated  $g$ -layer variant (*bottom*), on CIFAR-100. The  $g$ -layer model significantly reduces the KS error for all Top- $k$  classes.

tion seems to be able to find good learning hyper-parameters, mitigating overfitting when training (large) networks on a relatively small calibration set. We conclude that we can train  $g$ -layers effectively for different network architectures, using a range of hidden layers for various datasets.

**Number of hidden units** In this set of experiments we explore the number of hidden units used in the  $g$ -layer network and their relation to the calibration performance. For these experiments we train  $g$ -layers on the DenseNet models from CIFAR-10/100 and ILSVRC’12 (other networks/datasets are provided in the supplementary). The number of dense layers is varied, in the range 1 – 5, and the number of hidden units is set to  $H = h \times C + 2$ .

The results are in Fig 3. From these results we observe that in most cases the performance is stable across the number of hidden units and the number of layers. This shows that dense  $g$ -layers can be trained effectively over large number of parameters, when initialised with transparent layers and learning settings found by cross validation. From these results we do not see clear signs of overfitting.

The bad performance on the CIFAR-100 dataset, when using 2, 3 or 4 layers with  $h = 2$  can be explained by the failure to initialise correctly in a transparent manner. This is supported by the evaluation of the accuracy, where all other models obtain similar accuracy to the uncalibrated models, these two cases yield about random accuracy.

**Multi-class calibration** Our theory shows that  $g$ -layers, trained with NLL, optimize multi-class calibration, so far we have only evaluated the top-1 calibration. In this final set of experiments we show that our method indeed performs multi-class calibration.

In the first experiment, we use the ResNet 110 model on CIFAR-100 (other networks / datasets are provided in the

supplementary) and compare the uncalibrated network with a  $g$ -layer network (3 layer,  $h = 3$ ). In Fig 4 we show the calibration of the top-1 to top-4 classes, by the KS plots and the KS error for each class. From these results it is clear that (a)  $g$ -layers significantly reduce the KS-error for all top- $k$  classes; (b) that the top (few) classes have by far the most influence on multi-class calibration metrics, *e.g.* multi-class ECE (Kull et al. 2019) takes the average over all classes.

In the second experiment we evaluate the average top-10 KS error for all datasets and network architectures used. We compare the uncalibrated network with a  $g$ -layer network (3 layers,  $h = 3$ ). The results are in Table 3. From the results we observe that the calibrated network has a significant lower error, than the uncalibrated network. Based on these results from both experiments we conclude that  $g$ -layers indeed perform multi-class calibration.

## 7 Conclusion

The analysis in this paper gives broader conditions than previously known for a classifier such as a neural network to be correctly calibrated, ensuring that the network can be correctly calibrated during training, after early-stopping or through post-hoc calibration. This provides a theoretical basis for post-hoc calibration schemes.

In this paper we have also introduced  $g$ -layers, a post-hoc calibration network. It consists of a series of transparent dense prediction layers, concatenated to a pre-trained network. These  $g$ -layers are optimised using negative log likelihood training. Experimentally we have shown that  $g$ -layers obtain excellent calibration performance, both when evaluated for the Top-1 class as well as evaluated for multi-classes, across a large set of networks and datasets. We intend to study techniques to improve generalization with respect to calibration as a future work.

# Appendices

We first provide the proofs of the results of our main paper and then provide additional results.

## A Proofs of post-hoc calibration

### Lemma about change of variables

The following result will be useful. It is perhaps relatively obvious, but worth stating exactly.

**Lemma 4.** *Let  $X$  be a random variable with values in  $\mathcal{D}_X$  and  $f : \mathcal{D}_X \rightarrow \mathcal{D}_Z$  be a measurable function. Let  $h : \mathcal{D}_Z \rightarrow \mathbb{R}$  be a measurable function. If  $Z = f(X)$ , then*

$$E_{x \sim X} h(f(x)) = E_{z \sim Z} h(z) .$$

The proof follows from the definition of expected value, using a simple change of variables.

*Proof.* (sketch) The expectations may be written as

$$E_{x \sim X} h(f(x)) = \int h(f(x)) d\mu_X$$

$$E_{z \sim Z} h(z) = \int h(z) d\mu_Z ,$$

where  $\mu_X$  and  $\mu_Z$  are probability measures on  $\mathcal{D}_X$  and  $\mathcal{D}_Z$ . The desired equality then follows from a change of variables.  $\square$

The lemma can be given a more informal but more intuitive proof as follows. The expected value  $E_{x \sim X} h(f(x))$  can be computed by sampling  $x$  from  $X$  and taking the mean of the values  $h(f(x))$ . In the limit as the number of samples increases, this mean converges to the  $E_{x \sim X} h(f(x))$ .

Similarly,  $E_{z \sim Z} h(z)$  is obtained by sampling from  $Z$  and computing the mean of the values  $h(z)$ . However, random samples from  $Z$  are obtained by sampling  $x \sim X$  for then  $z = f(x)$  is a sample from the distribution  $Z$ . Hence, the two expectations give the same result.

### Submersions

We are interested in submersions from  $\mathbb{R}^m$  to  $\Delta^{n-1}$ , the standard open simplex.

**Proposition 5.** *Let  $q : \mathbb{R}^m \rightarrow \Delta^{n-1}$  be a submersion. If  $\sum_{y=1}^n w_y \partial q_y / \partial z_j = 0$ , then  $w_y$  is a constant for all  $y$ .*

*Proof.* Since  $\Delta^{n-1}$  has dimension  $n - 1$ , if  $q$  is a submersion, the Jacobian  $\partial q_y(z) / \partial z_j$  has rank  $n - 1$ . Since  $\sum_{y=1}^n q_y(z) = 1$ , taking derivatives gives  $\sum_{y=1}^n \partial q_y(z) / \partial z_j = 0$  for all  $j$ . Written in terms of matrices, with  $J = \partial q_y(z) / \partial z_j$  this says that  $\mathbf{1}^\top J = 0$ . Further, since  $J$  has rank  $n - 1$ , if  $\mathbf{w}^\top J = 0$  then  $\mathbf{w} = \alpha \mathbf{1}$ .

### Negative-logarithm loss and calibration

The following theorem is a known (in some form) property of the Negative-Logarithm cost function. The paper (Bishop 1994) gives the essential idea of the proof, but the theorem is not stated formally there.

**Theorem 6.** *Consider joint random variables  $(Z, Y)$ , taking values in  $\mathbb{R}^m$  and  $\mathcal{Y}$  respectively. Let  $q : \mathbb{R}^m \rightarrow \Delta^{n-1}$  be a submersion. Define the loss*

$$L(q, Z, Y) = -E_{(z,y) \sim (Z,Y)} \log(q_y(z)) .$$

If

$$\text{id} = \underset{g: \mathbb{R}^m \rightarrow \mathbb{R}^m}{\text{argmin}} L(q \circ g, Z, Y)$$

then

$$P(y | z) = q_y(z) .$$

*Proof.* The assumption in this theorem is that the value of the loss function cannot be reduced by applying some function  $g : \mathbb{R}^m \rightarrow \mathbb{R}^m$ . We investigate what happens to the function  $L(q, X, Y)$  when  $q$  is replaced by the composition  $q \circ g$ , where  $g : \mathbb{R}^m \rightarrow \mathbb{R}^m$  is some function. We compute

$$-L(q \circ g, Z, Y) = E_{(z,y) \sim (Z,Y)} \log(q_y(g(z)))$$

$$= \int \sum_{y=1}^n p(z, y) \log(q_y(g(z))) dz \quad (7)$$

We wish to optimize Eq 7 over  $g : \mathbb{R}^m \rightarrow \mathbb{R}^m$ . Let  $z \in \mathbb{R}^m$  and

$$z = (z_1, \dots, z_m) = (g_1(z), \dots, g_m(z)) = g(z) ,$$

which holds when  $g$  is the identity function.

The Euler-Lagrange equation concerns a functional of the form  $\int F(z, g, g') dz$ , and if derivatives  $g'$  do not appear in the functional, then the minimum (with respect to  $g$ ) is attained when the Euler-Lagrange equation holds for every  $j$ :

$$\frac{\partial F}{\partial g_j} = 0 .$$

Since here

$$F(z, g, g') = \sum_{y=1}^n p(z, y) \log(q_y(g(z))) ,$$

$$= \sum_{y=1}^n p(z, y) \log(q_y(g_1, \dots, g_m))$$

we compute

$$\frac{\partial F}{\partial g_j} = \sum_{y=1}^n p(z, y) \frac{\partial q_y / \partial z_j}{q_y(g_1, \dots, g_m)} = 0 ,$$

where  $\partial q_y / \partial z_j$  means the partial derivative of  $q_y$  with respect to its  $j$ -th component. This shows

$$\sum_{y=1}^n \frac{p(z, y)}{q_y(z)} \frac{\partial q_y}{\partial z_j} = 0 .$$

However, from Proposition 5, this implies that  $p(z, y) / q_y(z) = c$ , a constant, so  $p(z, y) = c q_y(z)$  for all  $y$ . However, since  $\sum_y q_y(z) = 1$  and  $\sum_y p(z, y) = p(z)$ , this gives  $p(z, y) = p(z) q_y(z)$ , or  $p(y | z) = q_y(z)$ , as required. This completes the proof of Theorem 6.  $\square$

A simple rewording of this theorem (changing the names of the variables) gives the following statement, which is essentially a formal statement of a result stated in (Bishop 1994).

**Corollary 7.** *Consider joint random variables  $(X, Y)$ , taking values in  $\mathcal{D}_X$  and  $\mathcal{Y}$  respectively, where  $\mathcal{D}_X$  is some Cartesian space. Let  $f : \mathcal{D}_X \rightarrow \Delta^{n-1}$  be a function. Define the loss*

$$L(f, X, Y) = -E_{(x,y) \sim (X,Y)} \log(f_y(x)) .$$

If

$$f = \underset{\hat{f}: \mathcal{D}_X \rightarrow \Delta^{n-1}}{\operatorname{argmin}} L(q \circ \hat{f}, X, Y)$$

then

$$P(y | x) = f_y(x) .$$

This corollary follows directly from Theorem 6 since if  $f$  minimizes the cost function over all functions, then it optimizes the cost over all functions  $f \circ g$ , where  $g : \mathcal{D}_X \rightarrow \mathcal{D}_X$ .

However, when  $\mathcal{D}_X$  is a high-dimensional space (such as a space of images), then it may be a very difficult task to find the optimum function  $f$  exactly. Fortunately, a much less stringent condition is enough to ensure the conclusion of the theorem, and that the network ( $f$ ) is calibrated.

**Corollary 8.** *Consider joint random variables  $(X, Y)$ , taking values in  $\mathcal{D}_X$  and  $\mathcal{Y}$  respectively. Let  $f : \mathcal{D}_X \rightarrow \mathbb{R}^m$ , and let  $q : \mathbb{R}^m \rightarrow \Delta^{n-1}$  be a submersion. Define the loss*

$$L(q \circ f, X, Y) = -E_{(x,y) \sim (X,Y)} \log(q_y(f(x))) .$$

If  $f$  is optimal with respect to recalibration, for this cost function, then  $P(y | f(x)) = q_y(f(x))$ .

*Proof.* Let  $Z = f(X)$ , and for any  $x$  define  $f(x) = z$ . Then, from lemma 4,

$$\begin{aligned} L(q \circ f, X, Y) &= -E_{(x,y) \sim (X,Y)} \log(q_y(f(x))) \\ &= -E_{(z,y) \sim (Z,Y)} \log(q_y(z)) \\ &= L(q, Z, Y) . \end{aligned}$$

Then, according to Theorem 6, if replacing  $q$  by  $q \circ g$  will not decrease the value of the loss function (which is the definition that  $f$  is optimal with respect to recalibration), we may conclude that

$$P(y | z) = q_y(z) .$$

as required.  $\square$

## B Multiclass and classwise calibration

We make the usual assumption of random variables  $X$  and  $Y$ . Suppose that a function  $f : \mathcal{D}_X \rightarrow \Delta^{n-1}$  is multiclass calibrated, which means that  $P(y | z) = z_y$ , where  $z = f(x)$ . We wish to show that it is classwise calibrated, meaning  $P(y | z_y) = z_y$ , and also that it is calibrated for top- $r$  and within-top- $r$  calibration. It was stated in (Kull et al. 2019) that classwise calibration, and calibration for the top class are “weaker” concepts of calibration, but no justification was given there. Hence, we fill that gap in the theorem below.

The proof is not altogether trivial, since certainly  $P(y | z_y)$  is not equal to  $P(y | z)$  in general. Neither does it follow from the fact that  $Z = z$  implies  $Z_y = z_y$ .

First, we change notation just a little. Let  $\hat{y}$  be the so-called  $n$ -dimensional one-hot vector of  $y$ , namely an indicator vector such that  $\hat{y}_k = 1$  if  $y = k$  and 0 otherwise. Then the condition for multi-class calibration is

$$P(\hat{y}_y = 1 | z_y = \sigma) = \sigma$$

**The top- $r$  prediction.** We wish also to talk about calibration of the top-scoring class predictions. Suppose a classifier  $f$  is given with values in  $\Delta^{n-1}$  and let  $y$  be the ground truth label. Let us use  $z^r$  to denote the  $r$ -th top score (so  $z^1$  would denote the top score). Note that an upper index, such as in  $z^r$  here represents the  $r$ -th top value, whereas lower indices, such as  $z_y$  represent the  $y$ -th class. Similarly, define  $\hat{y}^r$  to be 1 if the  $r$ -th top predicted class is the correct (ground-truth) choice, and 0 otherwise. The network is calibrated for the top- $r$  predictor if for all scores  $\sigma$ ,

$$P(\hat{y}^r = 1 | z^r = \sigma) = \sigma . \quad (8)$$

In words, the conditional probability that the top- $r$ -th choice of the network is the correct choice, is equal to the  $r$ -th top score.

Similarly, one may consider probabilities that a datum belongs to one of the top- $r$  scoring classes. The classifier is calibrated for being within-the-top- $r$  classes if

$$P(\sum_{s=1}^r \hat{y}^s = 1 | \sum_{s=1}^r z^s = \sigma) = \sigma . \quad (9)$$

Here, the sum on the left is 1 if the ground-truth label is among the top  $r$  choices, 0 otherwise, and the sum on the right is the sum of the top  $r$  scores.

**Theorem 9.** *Suppose random variables  $X$  and  $Y$  defined on  $\mathcal{D}_X$  and  $\mathcal{Y}$  respectively, and let  $f : \mathcal{D}_X \rightarrow \Delta^{n-1}$  be a measurable function. Suppose that  $P(y | z) = z_y$ , where  $z = f(x)$ . Then  $f$  is classwise calibrated, and also calibrated for top- $r$  and within-top- $r$  classes, as defined by Eq 8 and Eq 9.*

*Proof.* We assume that  $f$  is multiclass calibrated, so that  $P(\hat{y}_y = 1 | z) = z_y$ . First, we observe that

$$P(\hat{y}_y = 1, z) = P(\hat{y}_y = 1 | z) P(z) = z_y P(z) . \quad (10)$$

Then,

$$\begin{aligned} P(\hat{y}_y = 1 | z_y = \sigma) &= P(\hat{y}_y = 1, z_y = \sigma) / P(z_y = \sigma) \\ &= \int_{z_y = \sigma} P(\hat{y}_y = 1, z) dz / P(z_y = \sigma) \end{aligned}$$

where the integral marginalizes over all values of  $z$  with  $y$ -th entry equal to  $\sigma$ . Continuing, using Eq 10 gives

$$\begin{aligned} P(\hat{y}_y = 1 | z_y = \sigma) &= \int_{z_y = \sigma} z_y P(z) dz / P(z_y = \sigma) \\ &= z_y \int_{z_y = \sigma} P(z) dz / P(z_y = \sigma) \\ &= z_y P(z_y = \sigma) / P(z_y = \sigma) = z_y \end{aligned}$$

which proves that  $f$  is classwise calibrated.

Next, we show that  $f$  is top- $r$  calibrated. The proof is much the same, using top indices rather than lower indices. Analogously to Eq 10, we have

$$P(\hat{y}^r = 1, z) = P(\hat{y}^r = 1 | z) P(z) = z^r P(z). \quad (11)$$

This equation uses the equality  $P(\hat{y}^r = 1 | z) = z^r$ . To see this, fix  $z$ , and let  $y$  be the index of the  $r$ -th highest entry of  $z$ . Then  $z^r = z_y$  and  $\hat{y}^r = \hat{y}_y$ . Then  $P(\hat{y}^r = 1 | z) = P(\hat{y}_y = 1 | z) = z_y = z^r$ .

Then,

$$\begin{aligned} P(\hat{y}^r = 1 | z^r = \sigma) &= P(\hat{y}^r = 1, z^r = \sigma) / P(z^r = \sigma) \\ &= \int_{z^r = \sigma} P(\hat{y}^r = 1, z) dz / P(z^r = \sigma) \\ &\stackrel{\text{Eq 11}}{=} z^r \int_{z^r = \sigma} P(z) dz / P(z^r = \sigma) \\ &= z^r P(z^r = \sigma) / P(z^r = \sigma) \\ &= z^r. \end{aligned}$$

Here, the integral is over all  $z$  such that  $z^r = \sigma$ . This shows that  $f$  is top- $r$  calibrated.

Finally, we prove within-top- $r$  calibration. Refer to Eq 9, let  $\sigma$  be fixed, and let  $z$  be some vector such that  $\sum_{s=1}^r z^s = \sigma$ . Since for  $s = 1, \dots, r$  the events  $\hat{y}^s = 1$  are mutually exclusive, it follows that

$$P(\sum_{s=1}^r \hat{y}^s = 1 | z) = \sum_{s=1}^r P(\hat{y}^s = 1 | z) = \sum_{s=1}^r z^s = \sigma$$

This equality  $P(\sum_{s=1}^r \hat{y}^s = 1 | z) = \sigma$  will hold for any  $z$  such that  $\sum_{s=1}^r z^s = \sigma$ . It follows that

$$P(\sum_{s=1}^r \hat{y}^s = 1 | \sum_{s=1}^r z^s = \sigma) = \sigma,$$

as required.

Note the following justification for this last step. If some random variables  $A$  and  $Z$  satisfy  $P(A = a | Z = z) = \sigma$  (a constant) for all  $z$  in some class  $C$ , then  $P(A = a | z \in C) = \sigma$ . For, the assumption implies that  $P(A = a, Z = z) = \sigma P(Z = z)$ . Now, integrating for  $z \in C$  gives  $P(A = a, Z \in C) = \sigma P(Z \in C)$ , and hence  $P(A = a | Z \in C) = \sigma$ .  $\square$

What this theorem is saying, for instance, is that the probability that the correct classification lies within the top 2 (or  $r$ ) scoring classes, given that the sum of these two scores is  $\sigma$ , is equal to the sum of the two top scores.

The theorem can easily be extended to any set of classes, to show that if the classifier  $f$  is multiclass calibrated and  $S$  is any set of labels, that

$$P(\sum_{s \in S} \hat{y}^s = 1 | \sum_{s \in S} z^s = \sigma) = \sigma, \quad (12)$$

and

$$P(\sum_{s \in S} \hat{y}_s = 1 | \sum_{s \in S} z_s = \sigma) = \sigma. \quad (13)$$

## C Additional Results

In this section we provide additional results complementary to the results in the main paper.

For our experimental validation we calibrate deep convolutional neural networks trained on CIFAR-10/CIFAR-100 (Krizhevsky 2009), SVHN (Netzer et al. 2011) and ILSVRC'12 (Russakovsky et al. 2015) datasets. For the base network  $f$  we use pre-trained models of different architectures: ResNet (He et al. 2016), ResNet Stochastic Depth (Huang et al. 2016), DenseNet (Huang et al. 2017), and Wide ResNet (Zagoruyko and Komodakis 2016). For these experiments we use the pre-trained models also used in (Kull et al. 2019)<sup>2</sup>. We train the proposed  $g$ -layers on the validation set (not used for training base networks) which we denote *calibration set*. The models are then evaluated on the unseen test set.

### Calibration Error and Accuracy

For this set of experiments, we train  $g$ -layers with different number of dense layers, in the range from 1–5. The size of the hidden  $g$ -layers is fixed to 3 times the number of classes in the dataset plus 2, resulting in, 32, 302, and 3002 for CIFAR-10/SVHN, CIFAR-100, and ILSVRC'12 respectively. This relative large number is required for the transparent initialisation, which requires the number of dense units to be larger than double the number of classes. In practice this means that the number of weights in  $g$ -layers scale cubic with the number of classes, *e.g.* the 3-layer network for ILSVRC'12 contains 15M weights, while the 4-layer network has 24M.

The hyper-parameters for learning (learning rate and weight decay) are determined using 5-fold cross validation on the calibration set. The best results are used to train the  $g$ -layers on the full calibration set. We do cross validation for the single layer and 3 layer  $g$ -layer network, and use the parameters found for the 3 layer network also for  $\{2, 4, 5\}$  layer networks. For all  $g$ -layer models we use early stopping based on the negative log-likelihood of the current training set.

**Results** In this set of experiments we compare  $g$ -layer calibration to several other calibration methods, including: (1) Temperature scaling (Guo et al. 2017); (2) MS-ODIR (Kull et al. 2019); and (3) Dir-ODIR (Kull et al. 2019).

The results are presented in Table A.1 and Table A.2, reporting:

1. KS error (Gupta et al. 2021) in Table A.1a;
2. Classification accuracy in Table A.1b;
3. Brier score in Table A.1c;
4. Expected Calibration error in Table A.2a;
5. Average top-5 KS error Table A.2b; and
6. Average top-10 KS error Table A.2c.

From the Table A.1b we conclude that calibration does not hurt classification accuracy. The accuracy of the different models remains within  $\pm 0.1$  absolute percent point of the accuracy of the uncalibrated network.

Based on all results in Table A.1 and Table A.2 we conclude that the proposed  $g$ -layers provide effective calibrated models over a wide range of network depths.

<sup>2</sup>Pre-trained models are obtained from: [https://github.com/markus93/NN\\_calibration](https://github.com/markus93/NN_calibration).

Dataset	Base Network	Unc	TS	MS	Dir	<i>g</i> -Layers				
						D1	D2	D3	D4	D5
CIFAR-10	ResNet 110	4.751	<b>0.917</b>	0.988	1.076	0.924	0.990	0.954	1.116	1.066
	ResNet 110 SD	4.103	0.362	0.331	0.368	0.317	0.378	0.342	0.307	<b>0.188</b>
	Wide ResNet 32	4.476	0.296	<b>0.284</b>	0.313	0.320	0.296	0.351	0.337	0.420
	DensNet 40	5.493	0.900	0.897	0.969	0.911	1.026	<b>0.669</b>	1.679	1.377
SVHN	ResNet 152 SD	0.853	<b>0.553</b>	0.572	0.588	0.593	0.561	0.579	0.588	0.564
CIFAR-100	ResNet 110	18.481	1.489	2.541	2.335	1.359	1.618	<b>0.526</b>	1.254	-
	ResNet 110 SD	15.833	0.748	2.158	1.901	<b>0.589</b>	1.165	0.848	0.875	-
	Wide ResNet 32	18.784	1.130	2.821	2.000	0.831	<b>0.757</b>	1.900	0.857	-
	DensNet 40	21.157	0.305	2.709	0.775	0.249	<b>0.188</b>	0.199	0.203	-
ILSVRC'12	ResNet 152	6.544	0.792	5.355	4.400	0.776	<b>0.755</b>	0.849	0.757	-
	DensNet 161	5.721	<b>0.744</b>	4.333	3.824	0.881	1.091	0.780	1.105	-

(a) Calibration error on the test set, measured with KS error (Top-1 in %).

Dataset	Base Network	Unc	TS	MS	Dir	<i>g</i> -Layers				
						D1	D2	D3	D4	D5
CIFAR-10	ResNet 110	<b>93.6</b>	<b>93.6</b>	93.5	93.5	<b>93.6</b>	93.5	93.5	93.5	93.4
	ResNet 110 SD	94.0	94.0	<b>94.2</b>	<b>94.2</b>	<b>94.2</b>	94.1	94.1	94.1	94.0
	Wide ResNet 32	93.9	93.9	<b>94.2</b>	<b>94.2</b>	<b>94.2</b>	<b>94.2</b>	94.1	94.1	94.0
	DensNet 40	92.4	92.4	92.5	92.5	<b>92.6</b>	92.4	92.4	92.3	92.3
SVHN	ResNet 152 SD	<b>98.2</b>	<b>98.2</b>	98.1	<b>98.2</b>	<b>98.2</b>	<b>98.2</b>	<b>98.2</b>	<b>98.2</b>	98.1
CIFAR-100	ResNet 110	71.5	71.5	<b>71.6</b>	<b>71.6</b>	71.5	71.5	71.5	71.5	-
	ResNet 110 SD	72.8	72.8	<b>73.5</b>	73.1	73.0	72.9	73.2	73.2	-
	Wide ResNet 32	73.8	73.8	<b>74.0</b>	<b>74.0</b>	73.8	73.9	73.9	73.8	-
	DensNet 40	70.0	70.0	<b>70.4</b>	70.2	70.0	70.1	70.2	70.2	-
ILSVRC'12	ResNet 152	<b>76.2</b>	<b>76.2</b>	76.1	<b>76.2</b>	<b>76.2</b>	<b>76.2</b>	<b>76.2</b>	<b>76.2</b>	-
	DensNet 161	77.0	77.0	<b>77.2</b>	<b>77.2</b>	77.0	77.1	77.0	77.0	-

(b) Classification accuracy on the test set, measured with top-1 accuracy (in %).

Dataset	Base Network	Unc	TS	MS	Dir	<i>g</i> -Layers				
						D1	D2	D3	D4	D5
CIFAR-10	ResNet 110	1.102	0.979	<b>0.975</b>	0.976	0.979	0.976	0.978	0.983	0.988
	ResNet 110 SD	0.981	0.874	<b>0.866</b>	0.867	<b>0.866</b>	0.870	0.875	0.875	0.887
	Wide ResNet 32	1.047	0.924	0.890	0.888	0.890	<b>0.887</b>	0.896	0.897	0.900
	DensNet 40	1.274	1.100	<b>1.096</b>	1.097	1.099	1.098	1.102	1.113	1.121
SVHN	ResNet 152 SD	0.297	<b>0.291</b>	0.298	0.293	<b>0.291</b>	<b>0.291</b>	<b>0.291</b>	0.292	0.293
CIFAR-100	ResNet 110	0.453	0.392	<b>0.391</b>	<b>0.391</b>	0.392	0.392	0.392	0.393	-
	ResNet 110 SD	0.418	0.367	<b>0.361</b>	0.363	0.365	0.366	0.365	0.364	-
	Wide ResNet 32	0.432	0.355	<b>0.351</b>	0.354	0.355	0.354	0.354	0.354	-
	DensNet 40	0.491	0.401	<b>0.400</b>	<b>0.400</b>	0.401	<b>0.400</b>	0.401	0.401	-
ILSVRC'12	ResNet 152	0.034	<b>0.033</b>	<b>0.033</b>	<b>0.033</b>	<b>0.033</b>	<b>0.033</b>	<b>0.033</b>	<b>0.033</b>	-
	DensNet 161	0.033	<b>0.032</b>	<b>0.032</b>	<b>0.032</b>	<b>0.032</b>	<b>0.032</b>	<b>0.032</b>	<b>0.032</b>	-

(c) Calibration error on the test set, measured with the Brier error (multiplied by constant 100).

Table A.1: Overview of calibration error and accuracy on the (unseen) test set – part 1.

Dataset	Base Network	Unc	TS	MS	Dir	<i>g</i> -Layers				
						D1	D2	D3	D4	D5
CIFAR-10	ResNet 110	4.750	1.132	1.052	1.144	1.130	<b>0.997</b>	1.348	1.152	1.219
	ResNet 110 SD	4.113	0.555	0.599	0.739	0.807	0.809	0.629	0.674	<b>0.503</b>
	Wide ResNet 32	4.505	0.784	0.784	0.796	<b>0.616</b>	0.661	0.634	0.669	0.670
	DensNet 40	5.500	0.946	1.006	1.095	1.101	1.037	<b>0.825</b>	1.729	1.547
SVHN	ResNet 152 SD	0.862	0.607	0.616	0.590	0.638	<b>0.565</b>	0.589	0.604	0.648
CIFAR-100	ResNet 110	18.480	2.380	2.718	2.896	2.396	2.334	<b>1.595</b>	1.792	-
	ResNet 110 SD	15.861	<b>1.214</b>	2.203	2.047	1.219	1.405	1.423	1.298	-
	Wide ResNet 32	18.784	1.472	2.821	1.991	1.277	<b>1.096</b>	2.199	1.743	-
	DensNet 40	21.156	0.902	2.709	0.962	0.927	0.644	0.562	<b>0.415</b>	-
ILSVRC'12	ResNet 152	6.543	2.077	5.353	4.491	2.025	2.051	<b>1.994</b>	2.063	-
	DensNet 161	5.720	1.942	4.333	3.926	1.952	1.978	<b>1.913</b>	1.931	-

(a) Calibration error on the test set, measured with ECE error (Top-1 in %).

Dataset	Base Network	Unc	TS	MS	Dir	<i>g</i> -Layers				
						D1	D2	D3	D4	D5
CIFAR-10	ResNet 110	1.870	<b>0.460</b>	0.481	0.481	0.473	0.479	0.477	0.499	0.463
	ResNet 110 SD	1.627	0.200	0.186	0.192	0.199	0.189	0.180	0.175	<b>0.145</b>
	Wide ResNet 32	1.759	0.202	0.193	0.192	<b>0.162</b>	0.174	0.203	0.191	0.218
	DensNet 40	2.168	0.386	0.382	0.408	0.401	0.424	<b>0.293</b>	0.663	0.562
SVHN	ResNet 152 SD	0.304	0.219	<b>0.217</b>	0.222	0.231	0.220	0.225	0.223	0.218
CIFAR-100	ResNet 110	5.874	0.829	1.024	0.977	0.794	0.857	<b>0.594</b>	0.711	-
	ResNet 110 SD	5.212	0.349	0.748	0.696	<b>0.288</b>	0.429	0.351	0.375	-
	Wide ResNet 32	6.223	0.599	1.005	0.780	0.516	<b>0.491</b>	0.817	0.558	-
	DensNet 40	6.950	0.243	0.871	0.353	0.210	<b>0.179</b>	0.254	0.292	-
ILSVRC'12	ResNet 152	2.078	0.570	1.691	1.535	0.569	<b>0.560</b>	0.565	0.561	-
	DensNet 161	1.847	0.531	1.385	1.356	0.563	0.614	<b>0.523</b>	0.616	-

(b) Calibration error on the test set, measured in average Top-5 KS error (in %).

Dataset	Base Network	Unc	TS	MS	Dir	<i>g</i> -Layers				
						D1	D2	D3	D4	D5
CIFAR-10	ResNet 110	1.066	0.275	0.277	0.283	0.283	0.285	0.283	0.291	<b>0.269</b>
	ResNet 110 SD	0.918	0.118	0.113	0.114	0.117	0.113	0.108	0.105	<b>0.088</b>
	Wide ResNet 32	0.995	0.123	0.119	0.117	<b>0.101</b>	0.107	0.121	0.114	0.127
	DensNet 40	1.234	0.225	0.223	0.239	0.236	0.249	<b>0.174</b>	0.387	0.325
SVHN	ResNet 152 SD	0.188	0.134	<b>0.133</b>	<b>0.133</b>	0.142	0.134	0.138	0.137	0.134
CIFAR-100	ResNet 110	3.299	0.462	0.579	0.540	0.443	0.488	<b>0.336</b>	0.401	-
	ResNet 110 SD	2.904	0.241	0.434	0.407	<b>0.210</b>	0.277	0.234	0.234	-
	Wide ResNet 32	3.459	0.348	0.574	0.445	0.304	<b>0.299</b>	0.462	0.338	-
	DensNet 40	3.877	0.181	0.514	0.219	0.158	<b>0.128</b>	0.169	0.183	-
ILSVRC'12	ResNet 152	1.155	0.329	0.942	0.839	0.329	<b>0.326</b>	0.329	0.333	-
	DensNet 161	1.040	0.316	0.783	0.751	0.334	0.363	<b>0.306</b>	0.361	-

(c) Calibration error on the test set, measured in average Top-10 KS error (in %).

Table A.2: Overview of calibration error and accuracy on the (unseen) test set – part 2.

## Top- $k$ KS Calibration Error

In this set of experiments we present the top- $k$  KS error for ResNet 110 on CIFAR-10 and CIFAR-100, and for ResNet 152 on ImageNet. We compare the uncalibrated network to a 3  $g$ -layer network with 32/302, 3002 hidden units per layer (for 10/100/1000 classes). The results are presented in Fig A.1.

## Number of parameters

In this set of experiments we vary the number of parameters in the  $g$ -layer networks by changing the number of layers and the number of dense units per class. We measure the KS error (top 1) and the accuracy. The results are in Fig A.2-Fig A.4.

## Layer Initialisation

In this last set of experiments we compare the initialisation of the layers, using transparent initialisation, which ensure an identity transformation, or with standard random initialisation (using Glorot initialisation (Glorot and Bengio 2010)).

For this comparison we use ResNet 110 for CIFAR-10 and CIFAR-100 and ResNet 152 for ImageNet, using a 3  $g$ -layer network with 3 hidden units per class (resulting in 32, 302, and 3002 hidden units respectively). For each model, after each training epoch, we compute the negative log-likelihood (NLL), KS error and accuracy for the train set and test set. Since our models use early stopping, we re-normalize the x-axis to range from 0 - 100% training progress (instead of the number of epochs). For the transparent model the hyper-parameters from the cross validation search, for the normal (random initialised) models we manually tune the learning rate to get decent performance. **Note** the goal of this experiment is to show the benefit of transparent initialisation for  $g$ -layer training, not to get the best accuracy when trained from random initialisation.

The results are in Fig A.5. From the results we observe that transparent initialisation ensures that the accuracy remains at the same level of the base network. This is in stark contrast with normal (random initialised) models, where the accuracy starts from random performance. Subsequently, it seems that the while the normal models are able to learn the correct classification, this comes at the cost of their calibration. Hence we conclude that for *calibration* with  $g$ -layers transparent initialisation is preferred.

## References

Bishop, C. M. 1994. Mixture density networks. Technical report, Aston University.

Buja, A.; Stuetzle, W.; and Shen, Y. 2005. Loss functions for binary class probability estimation and classification: Structure and applications. *Technical report*.

Chen, T.; Goodfellow, I.; and Shlens, J. 2015. Net2net: Accelerating learning via knowledge transfer. *arXiv preprint arXiv:1511.05641*.

Glorot, X.; and Bengio, Y. 2010. Understanding the difficulty of training deep feedforward neural networks. In *International Conference on Artificial Intelligence and Statistics*.

Guo, C.; Pleiss, G.; Sun, Y.; and Weinberger, K. Q. 2017. On calibration of modern neural networks. In *Proceedings of the 34th International Conference on Machine Learning-Volume 70*, 1321–1330. JMLR. org.

Gupta, K.; Rahimi, A.; Ajanthan, T.; Mensink, T.; Sminchisescu, C.; and Hartley, R. 2021. Calibration of Neural Networks using Splines. In *International Conference on Learning Representations*.

He, K.; Zhang, X.; Ren, S.; and Sun, J. 2016. Deep residual learning for image recognition. In *Computer Vision and Pattern Recognition*.

Huang, G.; Liu, Z.; Van Der Maaten, L.; and Weinberger, K. Q. 2017. Densely connected convolutional networks. In *Computer Vision and Pattern Recognition*.

Huang, G.; Sun, Y.; Liu, Z.; Sedra, D.; and Weinberger, K. 2016. Deep Networks with Stochastic Depth. In *European Conference on Computer Vision*.

Krizhevsky, A. 2009. Learning multiple layers of features from tiny images. Technical report, CIFAR.

Kull, M.; Nieto, M. P.; Kängsepp, M.; Silva Filho, T.; Song, H.; and Flach, P. 2019. Beyond temperature scaling: Obtaining well-calibrated multi-class probabilities with Dirichlet calibration. In *Neural Information Processing Systems*.

Kull, M.; Silva Filho, T.; and Flach, P. 2017. Beta calibration: a well-founded and easily implemented improvement on logistic calibration for binary classifiers. In *Artificial Intelligence and Statistics*.

Kumar, A.; Liang, P. S.; and Ma, T. 2019. Verified uncertainty calibration. In *Neural Information Processing Systems*.

Müller, R.; Kornblith, S.; and Hinton, G. E. 2019. When does label smoothing help? In *Neural Information Processing Systems*.

Naeini, M. P.; Cooper, G.; and Hauskrecht, M. 2015. Obtaining well calibrated probabilities using bayesian binning. In *Twenty-Ninth AAAI Conference on Artificial Intelligence*.

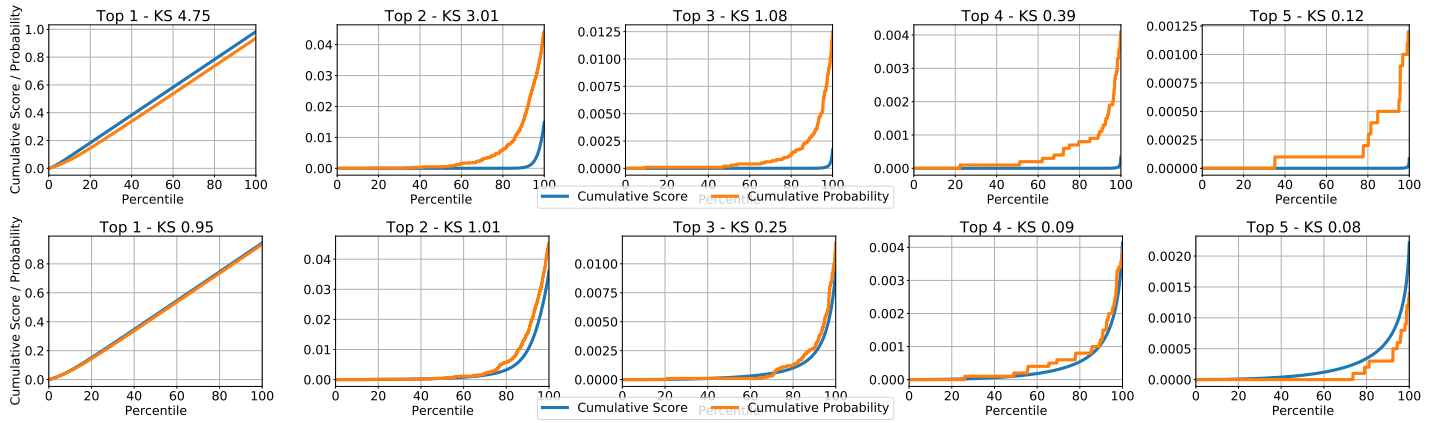
Netzer, Y.; Wang, T.; Coates, A.; Bissacco, A.; Wu, B.; and Ng, A. Y. 2011. Reading digits in natural images with unsupervised feature learning. In *NeurIPS Workshop on Deep Learning and Unsupervised Feature Learning*.

Platt, J.; et al. 1999. Probabilistic outputs for support vector machines and comparisons to regularized likelihood methods. *Advances in large margin classifiers*, 10(3): 61–74.

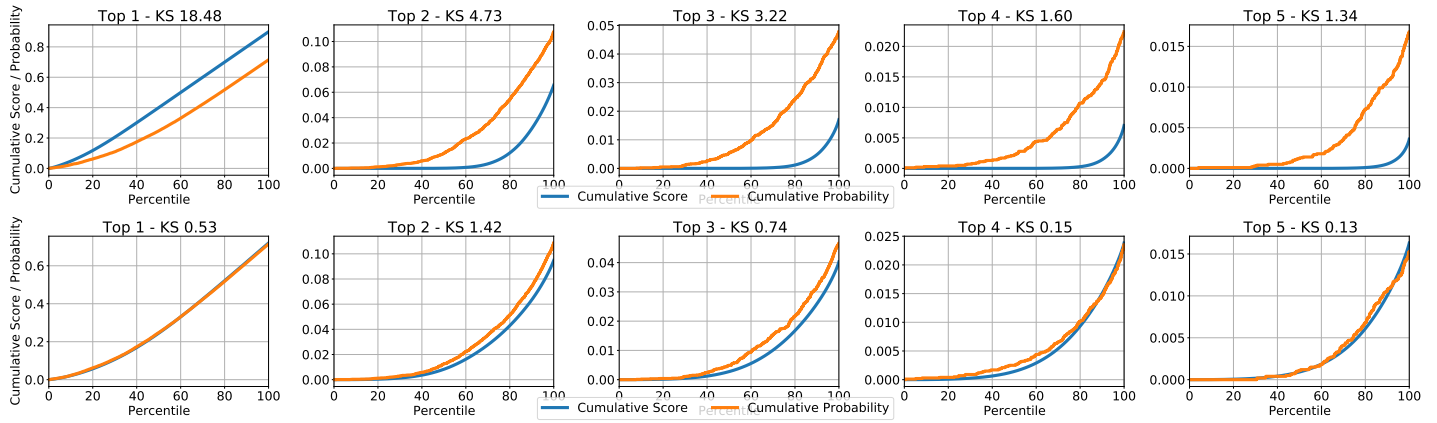
Rahimi, A.; Shaban, A.; Cheng, C.-A.; Boots, B.; and Hartley, R. 2020. Intra Order-preserving Functions for Calibration of Multi-Class Neural Networks. *arXiv preprint arXiv:2003.06820*.

Reid, M. D.; and Williamson, R. C. 2010. Composite binary losses. *Journal of Machine Learning Research*.

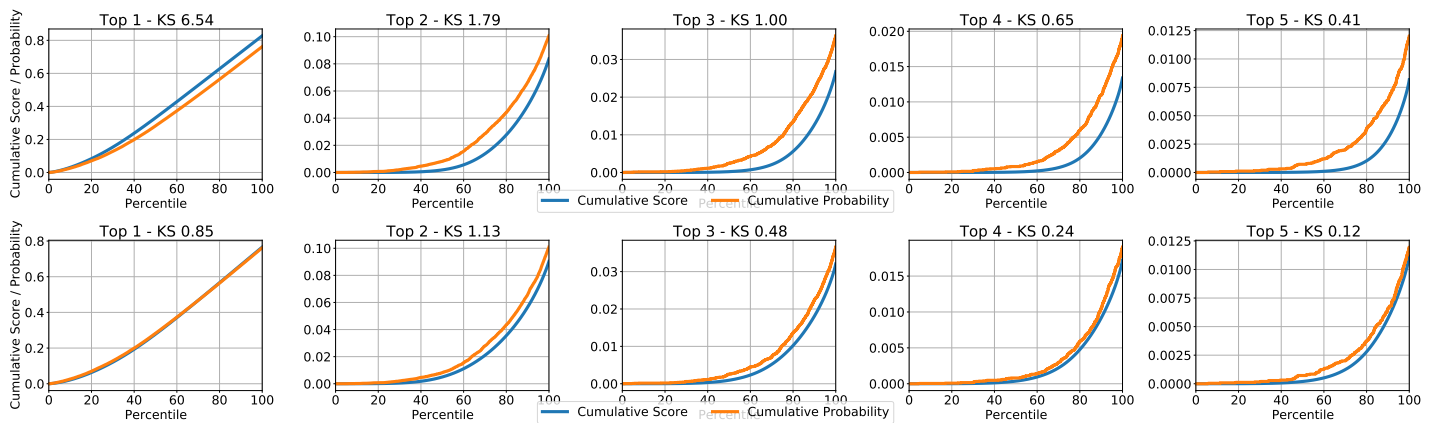
Russakovsky, O.; Deng, J.; Su, H.; Krause, J.; Satheesh, S.; Ma, S.; Huang, Z.; Karpathy, A.; Khosla, A.; Bernstein, M.; Berg, A. C.; and Fei-Fei, L. 2015. ImageNet Large Scale Visual Recognition Challenge. *International Journal on Computer Vision*, 115(3): 211–252.



(a) CIFAR-10 - ResNet 110: **top** Uncalibrated vs (bottom) Calibrated (3  $g$ -layer)

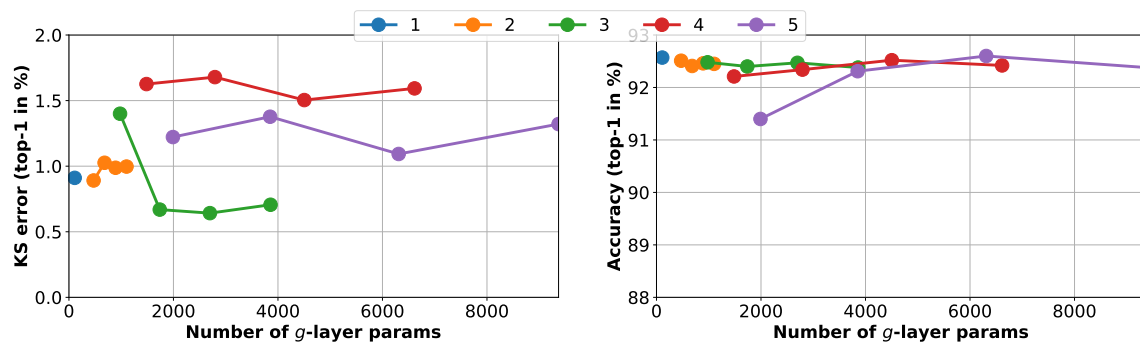


(b) CIFAR-100 - ResNet 110: **top** Uncalibrated vs (bottom) Calibrated (3  $g$ -layer)

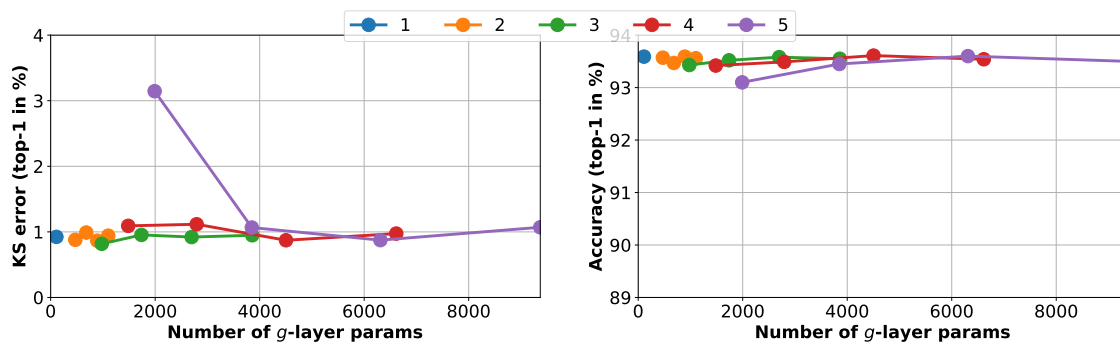


(c) ImageNet - ResNet 152: **top** Uncalibrated vs (bottom) Calibrated (3  $g$ -layer)

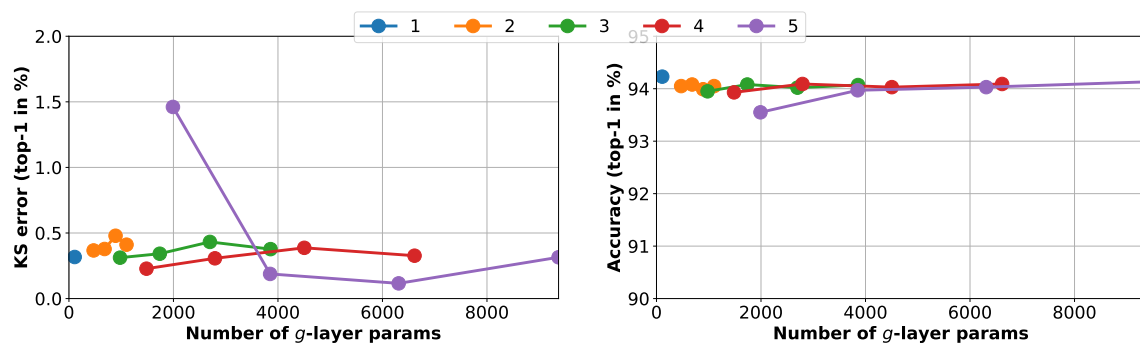
Figure A.1: Calibration error for top- $k$  KS error, with  $k = \{1, \dots, 5\}$ .



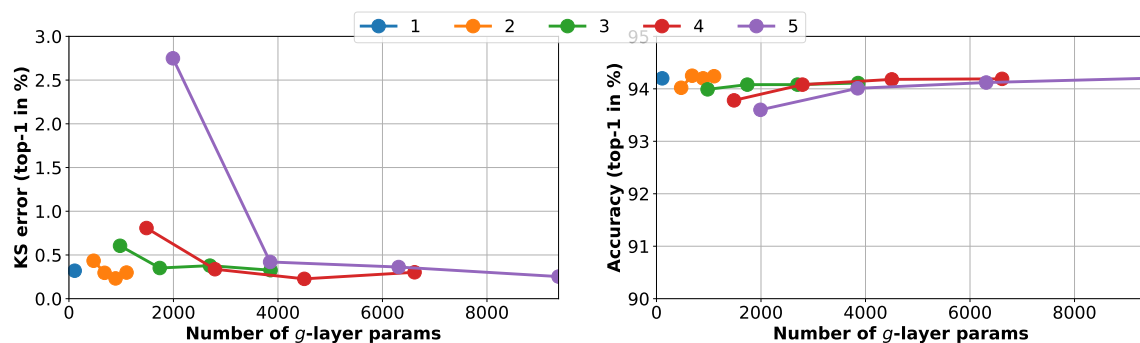
(a) CIFAR-10 – DenseNet 40



(b) CIFAR-10 – ResNet 110

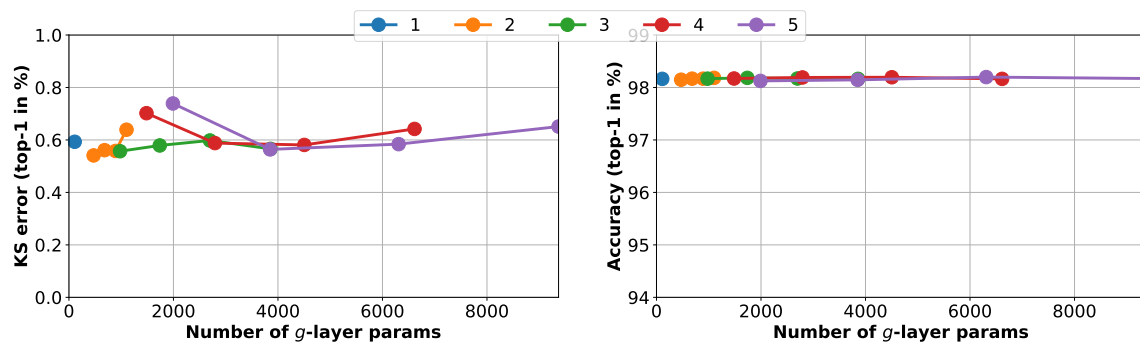


(c) CIFAR-10 – ResNet 110 SD

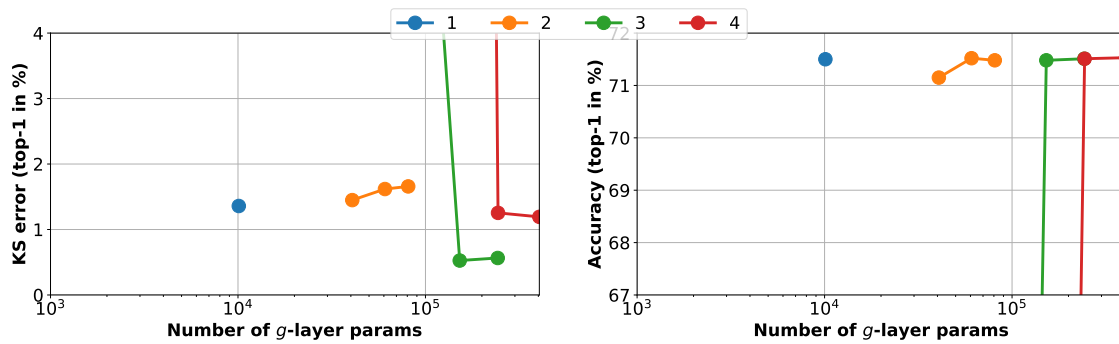


(d) CIFAR-10 – ResNet Wide 32

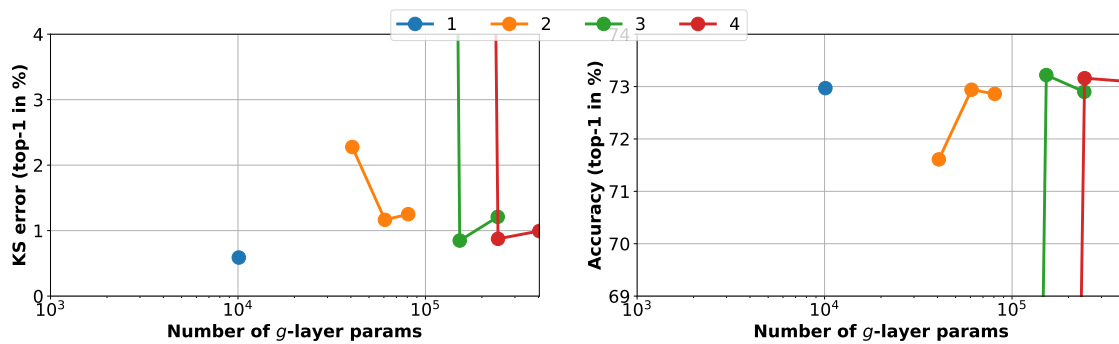
Figure A.2: Calibration (**left**) and Accuracy (**right**) as function of number of parameters. Number of parameters change by the number of dense layers, indicated by colored lines, and number of dense units per layer:  $\{2, 3, 4, 5\}$  units per class + 2.



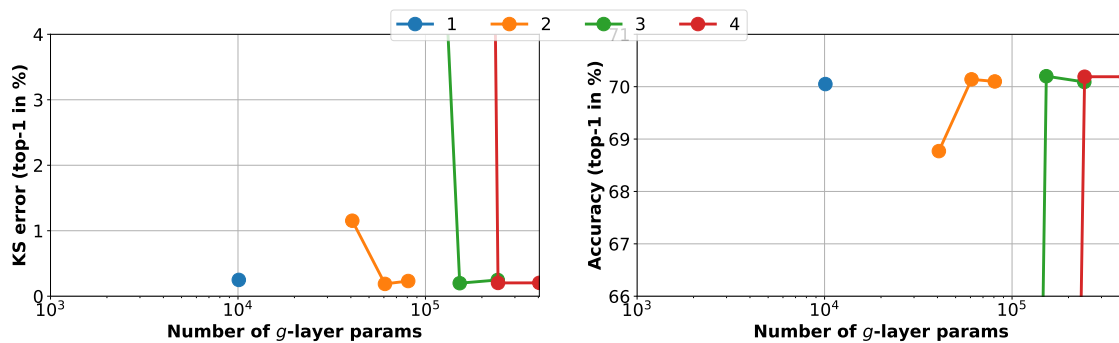
(a) SVHN – ResNet 152 SD



(b) CIFAR-100 – ResNet 110

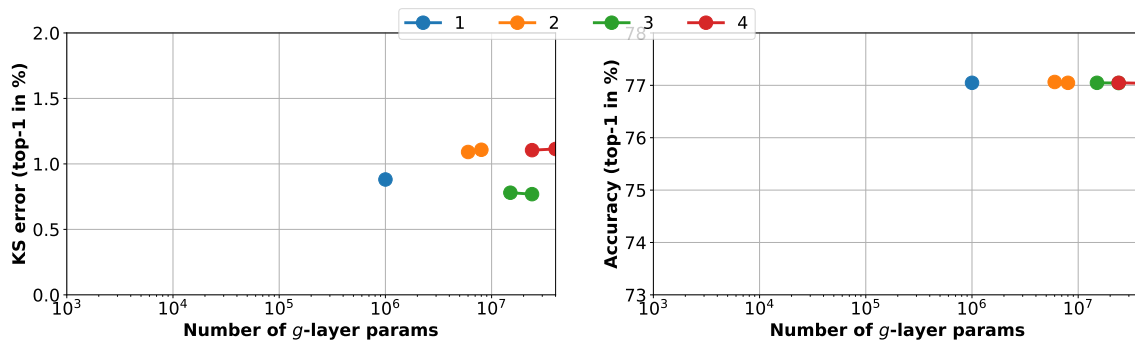


(c) CIFAR-100 – ResNet 110 SD

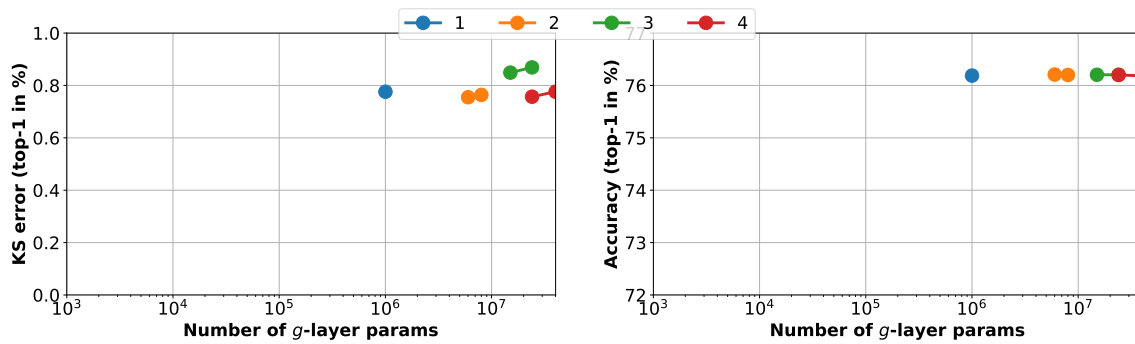


(d) CIFAR-100 – DenseNet 40

Figure A.3: Calibration (**left**) and Accuracy (**right**) as function of number of parameters. Number of parameters vary by the number of dense layers (colored lines), and number of dense units per layer:  $\{2, 3, 4\}$  units per class (SVHN also 5) + 2.



(a) ILSVRC'12 / ImageNet – DenseNet 161



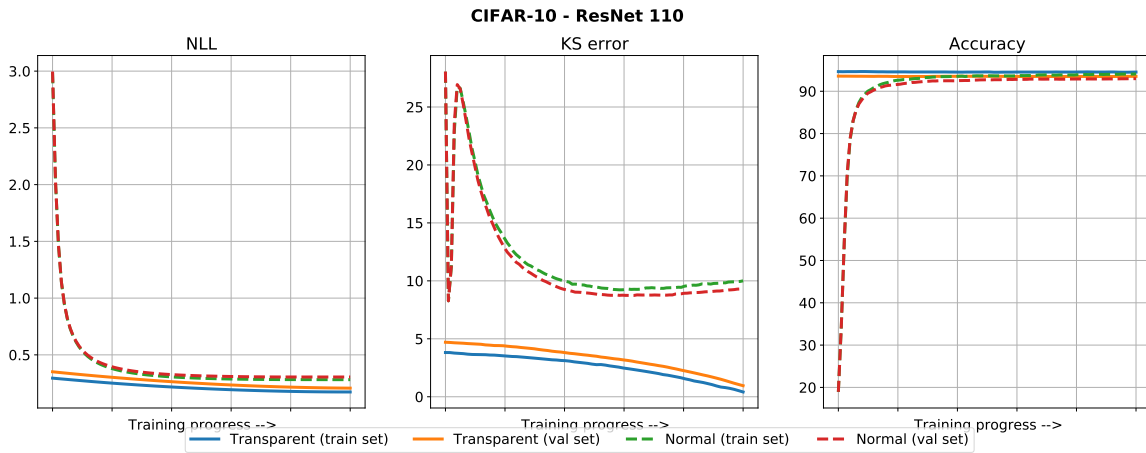
(b) ILSVRC'12 / ImageNet – ResNet 152

Figure A.4: Calibration (**left**) and Accuracy (**right**) as function of number of parameters. Number of parameters change by the number of dense layers (colors) and number of dense units per layer ( $\{3, 4\}$  times number of classes + 2).

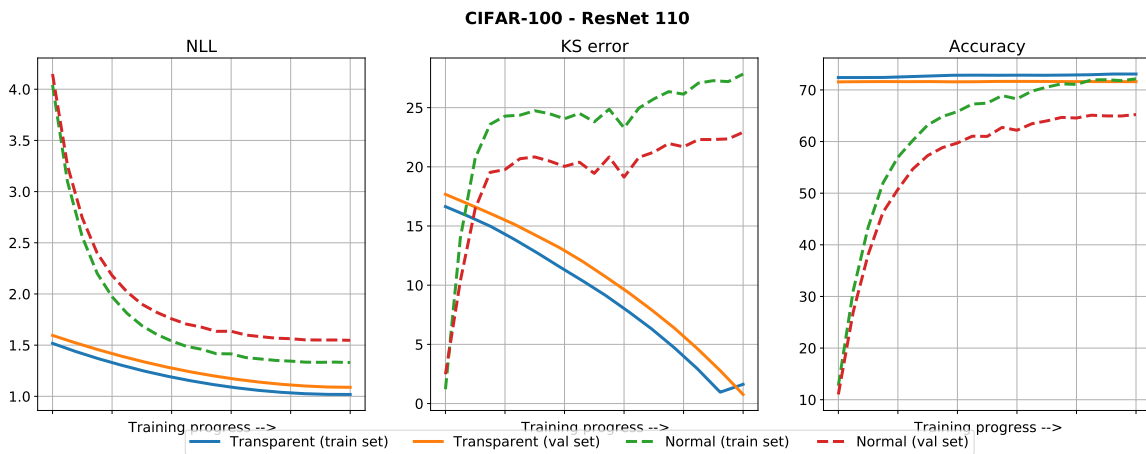
Zadrozny, B.; and Elkan, C. 2002. Transforming classifier scores into accurate multiclass probability estimates. In *Proceedings of the eighth ACM SIGKDD international conference on Knowledge discovery and data mining*, 694–699.

Zagoruyko, S.; and Komodakis, N. 2016. Wide residual networks. In *British Machine Vision Conference*.

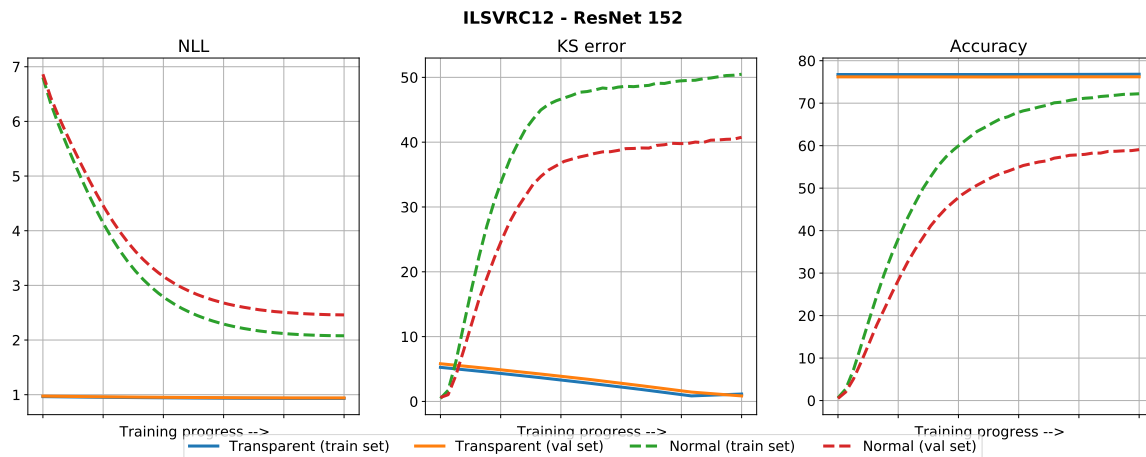
Zhang, H.; Cissé, M.; Dauphin, Y. N.; and Lopez-Paz, D. 2018. Mixup: Beyond Empirical Risk Minimization. In *International Conference on Learning Representations*.



(a) CIFAR-10 - ResNet 110: Transparent vs Normal layer initialisation



(b) CIFAR-100 - ResNet 110: Transparent vs Normal layer initialisation



(c) ImageNet - ResNet 152: Transparent vs Normal layer initialisation

Figure A.5: Negative log likelihood, KS error and accuracy measured during training of  $g$ -layer networks either initialised with transparent layers or with normal (random Glorot (Glorot and Bengio 2010)) initialisation.